



## Observed and predicted North American teleseismic delay times

Xiaoting Lou <sup>\*</sup>, Suzan van der Lee

*Department of Earth and Planetary Sciences, Northwestern University, Evanston, IL 60208, USA*

---

### ARTICLE INFO

#### Article history:

Received 16 February 2013

Received in revised form 28 November 2013

Accepted 30 November 2013

Available online xxxx

Editor: P. Shearer

#### Keywords:

North America

continent

plate tectonics

tomographic models

delay time

USArray

---

### ABSTRACT

Using a newly developed cross-correlation-based computer tool we measured absolute delay times of teleseismic *P* and *S* waves recorded by about 2000 broadband seismic stations from EarthScope's USArray, previous PASSCAL arrays, and additional permanent networks in North America. We estimate contributions to the delays from crustal structure, using various prior crustal models, and from event-side heterogeneity, using the delay time distribution itself. We then subtract these contributions from our measurements and map the average delay at each station location. We analyze these average delay times to investigate the structure of the North American mantle and formation of the North American continent. Mantle *S* delay times from stations west of the Rocky Mountains are 4.2 s larger than delay times from stations within the US portion of stable North America. Locally, *S* delays at Yellowstone are another 4 s larger than those west of Rocky Mountains. Decreasingly sharp delay time contrasts occur across the Rocky Mountains, the Appalachian Mountains, and on the southern edge of the North American Craton, respectively. These delay time gradients of various steepness broadly coincide with surface geological boundaries, but are offset to either side of these boundaries. Predictions of teleseismic *S* delays from twelve three-dimensional tomographic mantle *S* velocity models agree generally with observed delay time patterns, but underestimate the delays and advances to varying degrees. Tomographic models derived from different data than teleseismic arrival times predict similarly valid delays as models derived from teleseismic arrivals, while overestimating the smoothness of delay time patterns to varying degrees. We further utilize these tomographic models to predict and study the size and distribution of delay contributions from modeled heterogeneity in different depth ranges. This study shows that the 80–240 km depth range is the dominant contributor to delay time contrasts and variance. This depth range generally corresponds to asthenosphere in the western US and lithosphere in the central and eastern US. The average depth to which the observed delays require the central US lithosphere to extend is likely shallower than 240 km and consistent with the seismic bottom of lithosphere imaged in seismic-velocity models *not* derived from teleseismic delay times.

© 2013 Elsevier B.V. All rights reserved.

---

### 1. Introduction

Since the onset of EarthScope's USArray in 2004, unprecedented seismic data has become available as its Transportable Array (TA) moved eastward across the North American continent. This has allowed seismologists to better constrain the mantle structure beneath North America (Roth et al., 2008; Sigloch et al., 2008; Tian et al., 2009, 2011; Schmandt and Humpreys, 2010, 2011; James et al., 2011; Obrebski et al., 2010, 2011; Burdick et al., 2012, etc.). These models share common features, such as high velocity anomalies along Cascades related to the subducting Juan de Fuca Slab and pronounced low velocity anomalies beneath Yellowstone. The models have re-invigorated existing debates about the

links between Mesozoic and Cenozoic tectonic activity in western North America, and associated upper mantle heterogeneity, characterized by subduction of the Farallon and Kula Plates, and their trailing fragments (Atwater, 1970; Stock and Molnar, 1988; Lipman, 1992; Grand, 1994; Van der Lee and Nolet, 1997a; Sigloch and Mihalynuk, 2013). The models also address the interaction of subducted slab fragments with continental lithosphere, slab windows, uplift, and subsidence, extension (Coney and Reynolds, 1977; Atwater, 1989; Bally et al., 1989), rifting, and the cause of the Yellowstone hotspot. Because USArray's Transportable Array has not yet completed its data collection, many of these tomographic models cover the US mantle west of the Rocky Mountains well while showing large question marks for mantle structure east of the Rocky Mountains. Moreover, and despite similarities in the data and methods used, these tomographic models also show significant differences. In this paper, we assess these model differences by testing a dozen tomographic models against our observations of teleseismic *P* and *S* arrival time delays. These delays

\* Corresponding author.

E-mail addresses: [xlou@u.northwestern.edu](mailto:xlou@u.northwestern.edu) (X. Lou), [suzan@earth.northwestern.edu](mailto:suzan@earth.northwestern.edu) (S. van der Lee).

are extracted from seismograms from EarthScope's USArray, IRIS PASSCAL (Program for Array Seismic Studies of the Continental Lithosphere) arrays, and permanent seismic networks, sampling both the western and eastern US. We include tomographic models that were inferred, at least in part, from pre-Earthscope data and that span the entire continent or globe. In addition we make a particular attempt to characterize differences in mantle structure between different depth intervals and between west and east of the Rocky Mountains. The Rocky Mountains (Fig. 1a) separate the tectonically active part of North America to their west from a relatively stable part to their east (Bally et al., 1989; Whitmeyer and Karlstrom, 2007). The Archean Canadian Shield and the Proterozoic Interior Platform comprise the Precambrian North American Craton (Hoffman, 1988; Whitmeyer and Karlstrom, 2007) of central and eastern North America. The North American craton is flanked on the east side by the Paleozoic Appalachian Mountain chain and on the west side by the Cenozoic Rocky Mountain chain. Despite the current tectonic stability of North America east of the Rocky Mountains, some of its crustal and mantle structure remains enigmatic, such as beneath the intraplate New Madrid Seismic Zone (Braile et al., 1982), the failed Mid-continent Rift System (Van Schmus and Hinze, 1985), and the complex lithosphere–asthenosphere system beneath the eastern seaboard (Rychert et al., 2007; Van der Lee et al., 2008).

## 2. Data and method

### 2.1. Seismic data

We have used the Standard Order for Data (SOD; Owens et al., 2004) to download EarthScope and other seismic data from the IRIS Data Management Center (DMC) (Fig. 1b). The broadband seismograph networks used in this study are listed in the supplementary material (Table S1). We defined three virtual networks, USTA, XAXJ and XRNM, according to station operation time range. About two thousand broadband seismic stations within latitude 24–50°N and longitude 66–124°W were found by SOD for the time range between January 2005 and December 2011, some 1250 of which are EarthScope's TA stations. Other stations mainly are from EarthScope's Flexible Array (FA), the United States National Seismic Network (USNSN), and university-based networks such as Caltech's CI and Columbia University's LD. We refer to this set of stations as virtual array USTA. In total, 128,098 P and 126,917 S arrival times from 407 teleseismic earthquakes above  $M_w$  magnitude 6.0 recorded by USTA stations were measured (see Section 2.2). We also measured a total of 1384 P and 1155 S arrival times from 120 earthquakes above  $M_w$  magnitude 5.5 between February 1995 and March 1996 for MOMA (Missouri to Massachusetts, Fischer et al., 1996), ABBA (Adirondack Broadband Array) (<http://gretchen.geo.rpi.edu/roecker/adk95/adk95.html>) and a few USNSN and GSN/IU stations. We refer to this set of stations as virtual array XAXJ. Lastly, a total of 2496 P and 2316 S arrival times from 140 earthquakes above  $M_w$  magnitude 5.5 between May 2001 and December 2002 were measured for FLED (Florida to Edmonton, Wysession et al., 2000), and a few USNSN, IU and NM (Cooperative New Madrid Seismic Network) stations. We refer to this set of stations as virtual array XRNM. The epicenters of the teleseismic earthquakes measured in this study are shown in Fig. 1c. Earthquake origin times and hypocenter locations are from official catalogs in the preference order of EHB (Engdahl et al., 1998), ISC (International Seismological Centre, 2010), and USGS/NEIC PDE (<http://earthquake.usgs.gov/research/data/pde.php>).

### 2.2. Method for measuring teleseismic arrival times

To measure teleseismic body-wave arrival times we used a new Python-based tool named AIMBAT (Lou et al., 2013), which follows

the popular multi-channel cross-correlation (MCCC; VanDecar and Crosson, 1990) to estimate relative arrival times while providing an absolute reference time. The absolute time is provided by the user picking the phase onset in the stack of phase arrival waveforms after alignment by relative cross-correlation lag time. AIMBAT has a dynamic graphical user interface with options for data sorting and quality control. AIMBAT is easy to install and use, open-source, and publicly available, as described in Lou et al. (2013).

### 2.3. Relating delay times to mantle heterogeneity

Teleseismic body wave delay time variations are caused by seismic velocity perturbations near the source, the station, or the mantle in between. Because of geometrical spreading of teleseismic waves, the network footprint projected back to the source side diminishes, causing the effects of source-side anomalies to be largely the same for arrivals at all stations in the network. We correct the delay time measurements for station-side crustal structure and event-side anomalies as described in Sections 2.3.1 and 2.3.2, and the effects of Earth's ellipticity (Dziewonski and Gilbert, 1976). The resulting crust-and-event-corrected delay times reflect anomalies along the ray path segments in the mantle beneath the stations.

#### 2.3.1. Station-side crustal corrections

To isolate effects of mantle velocity variations on teleseismic body wave delay times, effects of crustal structure are estimated and subtracted from the delays. The Crust 2.0 model (Bassin et al., 2000) specifies 7-layer (ice, water, soft sediments, hard sediments, upper crust, middle crust and lower crust) one-dimensional crustal models on the  $2 \times 2^\circ$  global grid. Lowry and Pérez-Gussinyé (2011) jointly inverted seismic receiver functions, gravity and surface heat flow measurements for an optimally interpolated model of crustal thickness and  $V_p/V_s$  ratio for the western US. A subsequent update of this model (Lowry et al., 2013), which extends further east, was used here to correct delay times for Moho depth for each station. For stations not in the grid of Lowry's model, we used Moho depth from NA04 (Van der Lee and Frederiksen, 2005). Choosing iasp91 (Kennett and Engdahl, 1991) as the one-dimensional reference model, replacing its Moho depth by values from Lowry's model or NA04, adding the two sediment layers interpolated from Crust 2.0, and station elevation, we constructed one-dimensional crustal models for each station. Because of the near-vertical incidence of the ray paths of the measured delay times, we further approximated the crustal corrections by the excess vertical travel time through each station's crustal model. By subtracting these estimated crustal corrections from the measured delay times, the effects of crustal structure, including topography, sediments and Moho depth were diminished. The crustal corrections are not correlated in size with the uncorrected observed delay times. The uncorrected and corrected observed delay times have similar distributions and show similar geographic patterns, suggesting they are dominated by mantle signal.

#### 2.3.2. Event-side corrections

To formally separate the effects of source-side heterogeneity on the delay times from the effects of heterogeneity in the study region, we inverted the delay time data set for station and event terms in an approach similar to Frederiksen et al. (2013). A crust-corrected delay time measurement  $t_{ij}$  from the  $i$ -th of  $N$  stations and the  $j$ -th of  $M$  events can be expressed as:

$$t_{ij} = s_i + e_j, \quad (1)$$

where  $s_i$  ( $i = 1, \dots, N$ ) are the station-side mantle delay terms and  $e_j$  ( $j = 1, \dots, M$ ) represent event terms and common structure along the ray paths away from the study region and near the

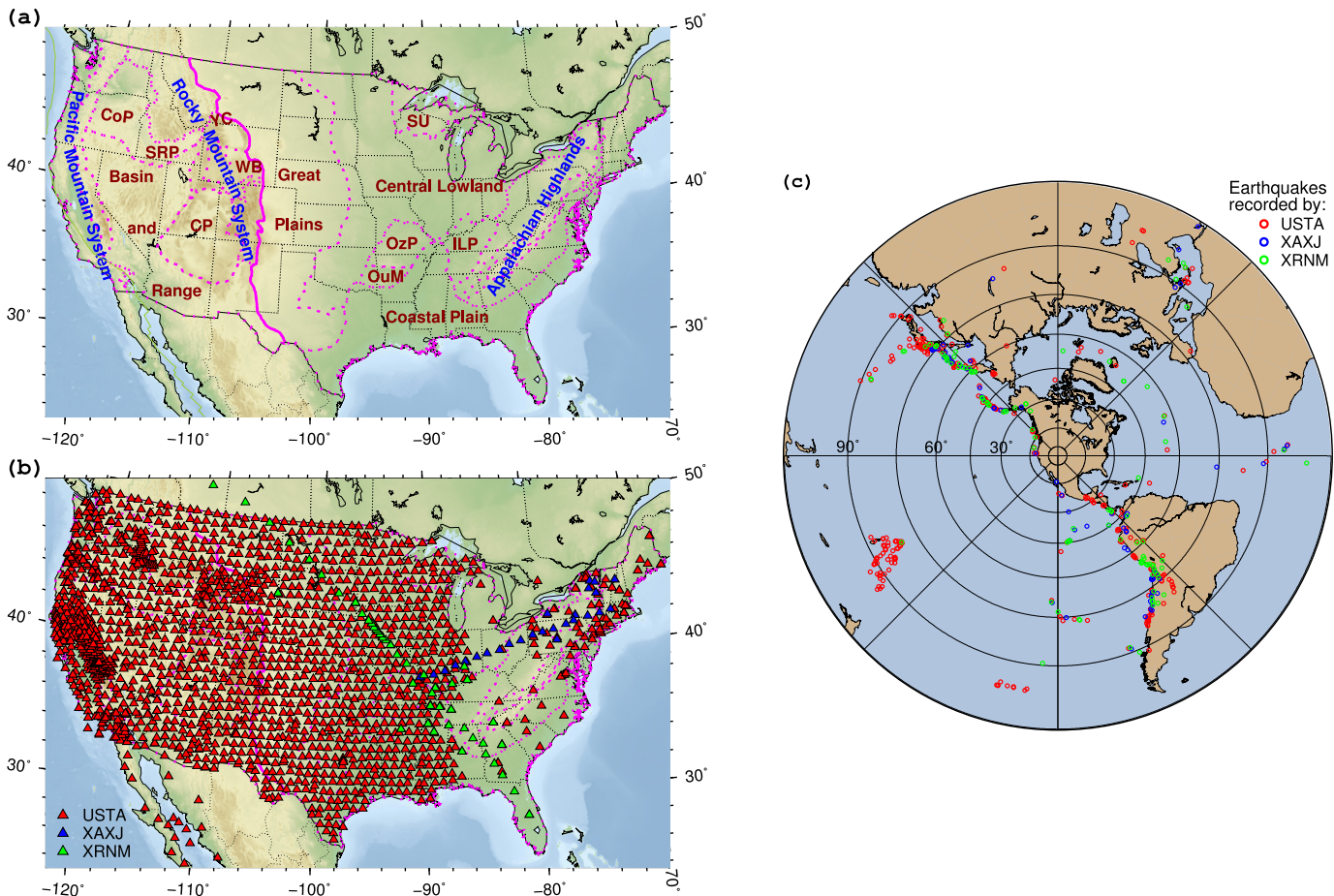


**Fig. 1.** (a) Geological provinces (<http://tapestry.usgs.gov/physiogr/physio.html>) and topography map of the US. Abbreviated names: CP (Colorado Plateaus), CoP (Columbia Plateau), SRP (Snake River Plain), YC (Yellowstone Caldera), WB (Wyoming Basin), SU (Superior Upland), OzP (Ozark Plateaus), OuM (Ouachita Mountains), and ILP (Interior Low Plateaus). The Pacific Mountain System includes the Pacific Border province and the Cascade–Sierra Mountains. The Rocky Mountain System consists of the Southern, Middle, Northern Rocky Mountains and the Wyoming Basin. The InterMontane Plateaus is comprised of the Columbia Plateau, the Colorado Plateau and the Basin and Range provinces. Solid purple line marks the boundary between the western and eastern US and divides all stations into two virtual networks RWW and RME. (b) Station locations for three virtual networks defined in this study: USTA stations between January 2005 and December 2011; XAXJ stations between February 1995 and March 1996; XRNM stations between May 2001 and December 2002. (c) Distribution of the measured teleseismic earthquakes recorded by USTA, XAXJ and XRNM stations, respectively. Hypocenter locations are from catalogs in the preference order of EHB, ISC and PDE.

source. If we invert the crust-corrected delay times  $t_{ij}$  for  $s_i$  and  $e_j$ , then the term  $s_i$  reflects the effects of the average mantle structure beneath the station.

In this study, we have measured 131,978  $P$  delays and 130,388  $S$  delays from 667 events and 1983 stations. The number of unknowns thus is  $N + M = 2660$ , which is much less than the number of delay measurements. The best fitting  $s_i$  and  $e_j$  were found by a least-squares method.

### 2.3.3. Station-side mantle delays

The event terms  $e_j$  are subtracted from the observed delays, which are already corrected for crustal structure, to expose the delays incurred in the mantle beneath the study region. The station-side mantle delay terms  $s_i$  reflect the portion of these mantle delays that is common for all rays converging at that station (Fig. 2a, b). This effective averaging of mantle delays is particularly sensitive to lithospheric and asthenospheric anomalies because these converging bundles of teleseismic ray paths span a width of only 150–300 km at a depth of 200 km. That width doubles at the top of the transition zone and is quadrupled in the lower mantle. This allows shallow heterogeneity of the same strength and scale as deeper heterogeneity, to have a stronger effect on the station-side mantle delays (or average station delay) than the deeper heterogeneity. Most of the ray paths to stations in

the US are either from the northwest or southeast. Consequently the station-side mantle delays would be more strongly affected by structures that stretch in the NW–SE direction rather than by perpendicular structures. However, analyzing observed delay times separately in up to four different azimuth ranges showed very similar mantle delay patterns, suggesting that the effects of non-uniform path coverage are minimal.

## 3. Results

### 3.1. Relative and absolute delay times

In traditional travel-time tomography, absolute delay times from hand picking can be imprecise, while relative delay times from cross-correlation have a higher precision but leave a region's average velocity structure unconstrained because an unknown mean delay time is removed for each earthquake. This also removes the effects of large-scale anomalies in the study region and can lead to heterogeneity in tomographic models being underestimated by over 20%. Owing to AIMBAT, our delay time measurements represent absolute delays without requiring time-consuming phase-picking.

Fig. 2a, b show the station-side mantle delays derived from crust-corrected absolute delay times as described in Section 2.3.2, which closely resemble the station-average of crust-corrected

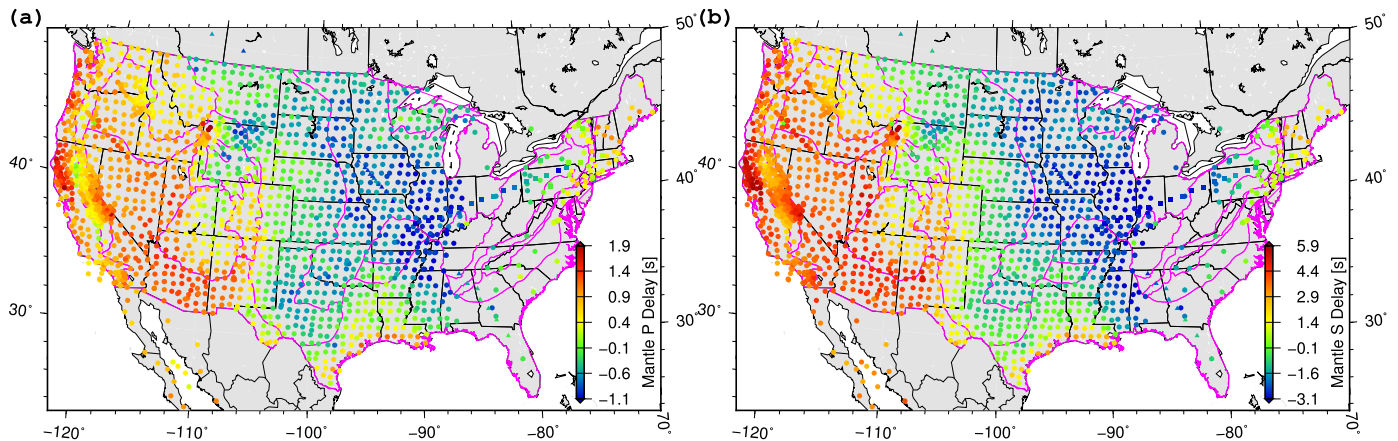


**Fig. 2.** Station-side mantle delays derived from crust-corrected absolute delay times as described in Section 2.3.2.

absolute delays. As expected from numerous previous studies, (e.g., Grand, 1994; Lee and Grand, 1996; Roth et al., 2008; Sigloch et al., 2008; Tian et al., 2009, 2011; Schmandt and Humphreys, 2010, 2011; James et al., 2011; Obrebski et al., 2010, 2011; Burdick et al., 2012), the regionally-averaged station delays differ in strength from one geological domain to another. The Wyoming Basin and northern Colorado Plateau are characterized by negative delays, which are surrounded by positive delays within the Basin and Range and southern Rocky Mountains, though flanked by fast arrivals east of the Rocky Mountains. The Snake River Plain is also delineated by positive delays. These delays exhibit a strong and sharp local maximum at two TA stations in Yellowstone National Park. Stations near the coast of Texas and Louisiana (Gulf Coastal Plain) exhibit positive delays.

### 3.2. Contrasts across the Rocky and Appalachian Mountains

Seismic velocity heterogeneity in the mantle is predominantly the result of thermal heterogeneity. However, thermally incompatible anomalies or sharp vertical and lateral contrasts in mantle lithospheric velocities can be indicators of chemical and/or other physical contrasts (Lee and Grand, 1996; Fischer et al., 2010). Bedle and van der Lee (2009) estimated that the lithospheric *S* velocity changes by at least 1% for every 100 km across the Rocky and Appalachian Mountain Fronts. A more regional study by Lee and Grand (1996) found this Rocky Mountain contrast in *S* velocity to be as high as 9% over about 600 km, which was deduced from teleseismic *S* delay times differing by 5 s over these 600 km. Lee and Grand (1996) inferred that at least part of this contrast would be caused by partial melt west of the Rocky Mountain Front. We also observe sharp contrasts across the Rocky Mountains in our delay time measurements.

Fig. 4 shows the variations of station-average crust-and-event-corrected absolute *S* delays along 6 profiles. Locations of the profiles are plotted in Fig. 3. We estimated delay time gradients from these and many more such profiles not plotted here. *S* delay contrast between the Southern Rocky Mountains and the Great Plains (TA profile Q, Fig. 4b) is about 3.5 s over 350 km, similar to Lee and Grand (1996). Further south, a *S* delay contrast of 5 s over 500 km between the Southern Basin and Range and the Great Plains (TA profile Z, Fig. 4c) presents a similar gradient over a broader region. Across the Northern Rocky Mountains, *S* delays decrease about 2 s over 200 km. *S* delay contrasts of 4 s over 300 km across the Middle Rocky Mountains (TA profile H, Fig. 4a) and 4 s over 350 km across the Wyoming Basin are stronger than elsewhere. Along the H profile (Fig. 4a), station TA.H17A stands out with a high *S* delay of 6.9 s. Nearby station US.LKWy (not shown) has an even larger *S* delay of 7.9 s. Both stations are in the Yellowstone Caldera.

Schmandt and Humphreys (2010) found the strongest lateral upper mantle *S* velocity gradient of 14.5% over <150 km between the Colorado Plateau and Great Basin in their tomographic model. Their high velocity body on the Colorado Plateau side of the gradient is imaged with a thickness of 65 km. Over 65 km, a 14.5% *S* velocity contrast would produce no more than two thirds of the 3.5 s delay contrast recorded in our delay times (Fig. 4b) over nearly 350 km, suggesting that even the strongest tomographically imaged gradient might be underestimating actual gradients.

The east–west seismic-velocity dichotomy typically imaged in global models is more complex when examined with the footprint of TA. The sharp transitions in delay times across the Rocky Mountains do not coincide with the surface geological boundary between the Rocky Mountains and the Great Plains. Some negative delay times are present west of the boundary in the Northern and Middle Rocky Mountains, and Wyoming Basin, while a sliver of positive delay times is present east of the boundary in the Southern Rocky Mountains and southern Basin and Range, running through eastern Colorado and eastern New Mexico, along the Rio Grande Rift.

In the east, *S* delays change more gradually across the Appalachian Mountains (Fig. 4e–f), but the gradient steepens near the Coastal Plain. According to Whitmeyer and Karlstrom (2007), the location of the Proterozoic Grenville Front is slightly west of the western boundary of the Appalachian Highlands. These teleseismic *S* delays thus confirm that the eastern edge of the North American craton is defined by Paleozoic orogens rather than Proterozoic ones (Bedle and van der Lee, 2009). In the northern Appalachians, *S* delays increase 3 s over 300 km along the MOMA profile from Proterozoic lithosphere in the midwest to Paleozoic margin in New England (Fig. 4e). In the southern Appalachians, *S* delays increase 2 s over 500 km along the FLED profile from the Great Plains to the Coastal Plain (Fig. 4f), which has a minimum near the profile center where the delay pattern is complicated around the Mid-continent Rift. French et al. (2009) found that receiver functions exhibit similar complexity.

In the south, the *S* delay contrast between the Interior Plains and the Coastal Plain (TA profile 36, Fig. 4d) is less sharp than both those across the Rocky and Appalachian Mountains. The transition of 2 s occurs over a much broader region, about 1000 km wide.

In summary, *S* delays within the Interior Plains are 3 to 5 s lower than the surrounding regions. Sharp contrasts are observed across both the Rocky and Appalachian Mountains, and the former are sharper than the latter. The delay contrast across the Rocky Mountains is offset to both west and east of the mountain front. *S* delay gradients range 1–1.3 s per 100 km on the west, 0.4–1 s per 100 km on the east, and 0.2 s per 100 km on the south side of the North American craton.

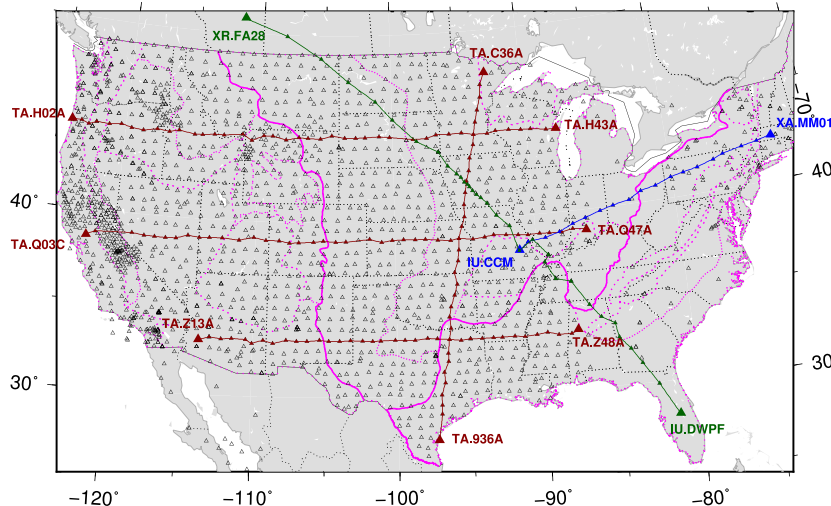


**Fig. 3.** Map of locations of the 6 profiles shown in Fig. 4. Solid purple lines roughly delineate the west, south, and east edges of the North American Craton.

### 3.3. Comparison between the Western and Eastern US

We define another virtual network RMW, which includes all stations to the west of the Rocky Mountain Front (solid purple line in Fig. 1a, b). Other stations are grouped into virtual array RME.

From 375 teleseismic earthquakes with both *P* and *S* measurements, 58,180 and 28,468 delay pairs are found for RMW and RME, respectively. The means of the absolute *P* and *S* delay times for RME are smaller than those for RMW, by 1.2 s for *P* and 4.2 s for *S*. This large difference indicates faster mantle beneath the eastern US, as imaged consistently in continental-scale and global models. Moreover, this difference is close to the 5+ s difference between stable continents and ocean islands, used by Jordan to argue for a deep tectosphere (Jordan, 1975), as well as to the 4.8 s difference in vertical travel time between *S* velocity models SNA and TNA (Grand and Helmberger, 1984) for the stable and western US upper mantles, respectively. The upper 175 km of the models, which corresponds to the seismic lithosphere in model SNA, contribute 3 s to this contrast. Our 4.2 s contrast would be incurred in the top 270 km of these two models, even though the models differ moderately down to 420 km, in accordance with Jordan's deep tectosphere. However, surface wave analyses (Cara, 1979; Van der Lee and Nolet, 1997b) have shown that the low, asthenospheric *S* velocities beneath the western US are significantly lower and confined to shallower depths than TNA's low velocities, which are inferred from body wave delays that represent more uniform depth integrals. Assuming such low asthenospheric velocities beneath RMW from more recent tomographic models, including NA04 and NA07 (Van der Lee and Frederiksen, 2005; Bedle and van der Lee, 2009), would produce the observed delay time contrast within the top 150 km. Confining the source of our 4.2 *S* delay contrast to the top 150 km would require an upper mantle velocity contrast of 17%. For comparison, extending the mantle source of the delays down to a depth of 250 km, would imply a velocity contrast of 9%. If these contrasts are entirely ascribed to temperature differences, the 17% contrast would imply a ~900 °C difference, while the 9% contrast would imply a ~600 °C difference (Cammarano et al., 2003). A temperature difference of 600 °C in the sub-Moho lithosphere is consistent with differences in heat flow between the Basin and Range and the mid-continent (Goes and van der Lee, 2002), which imply larger temperature differences at greater lithospheric depths. In this case, the widespread presence of water or partial melt would not be required. If water or partial melt is required based on other evidence (Dixon et al., 2004), the eastern US average lithosphere would have

to be proportionally thinner than 250 km. For example, if 6% *S* velocity contrast was explained by partial melt and/or water, then the eastern US lithosphere could be no thicker than 175 km on average. As a crude rule of thumb, about a dozen km of eastern lithosphere may be traded for a 1% water- or melt-induced *S*-velocity reduction in the west.

#### 3.3.1. Depth contribution of the delays

We predict *P* and *S* delay times from a suite of three-dimensional tomographic models listed below Fig. 5. Many of these models were compared by Pavlis et al. (2012) with his mantle discontinuity model derived from a plain wave migration inversion. Because of significant differences between the tomographic models they concluded that objective, quantitative evaluations of tomographic models are needed. Here we provide one such evaluation in that we compare the predicted delay times and their geographic patterns with our delay time measurements. We also investigate the relative contributions of different depth ranges to delay time patterns.

In the following we first compare the delay time patterns of the predicted average *S* delay per station (Fig. 5) and then their statistical distributions (Supplementary Fig. S2). The comparisons for *P* delays yielded similar observations and conclusions as those for their companion models' *S* delays and are not discussed in detail.

Model wUS11-S predicts observed *S* delays better than the other models. The model produces particularly good predictions for the central part of the study area, containing Yellowstone, the Wyoming Basin, the Colorado Plateau, and for the Gulf Coast. Model wUS11-S slightly underestimates the strength of delays on the west coast, the Northern Rocky Mountains, and large portions of the Central Lowland, which lie on the edges of the study region. Model DNA10-S predicts *S* delays well for the Colorado Plateau, Wyoming Basin, and Great Plains, but like NWUS11-S, underestimates the strength of delays elsewhere.

Model NA04 predicts delay times well along the northern US border, in the Basin and Range, in New England, and in the Great Plains, but underestimates delays in Yellowstone and the west coast, and overestimates the Central Lowland and Wyoming craton (which extends to the northeast from the Wyoming Basin and Yellowstone Caldera), and the eastern half of the Coastal Plain, including the Mississippi Embayment. Model NA07 predicts similar delay patterns as NA04 but does better in the Central Lowland, the Wyoming craton, and the west coast. Both models predict a respectable 75% of the large-scale delay contrast between the western US (RMW stations) and central US (RME stations minus the

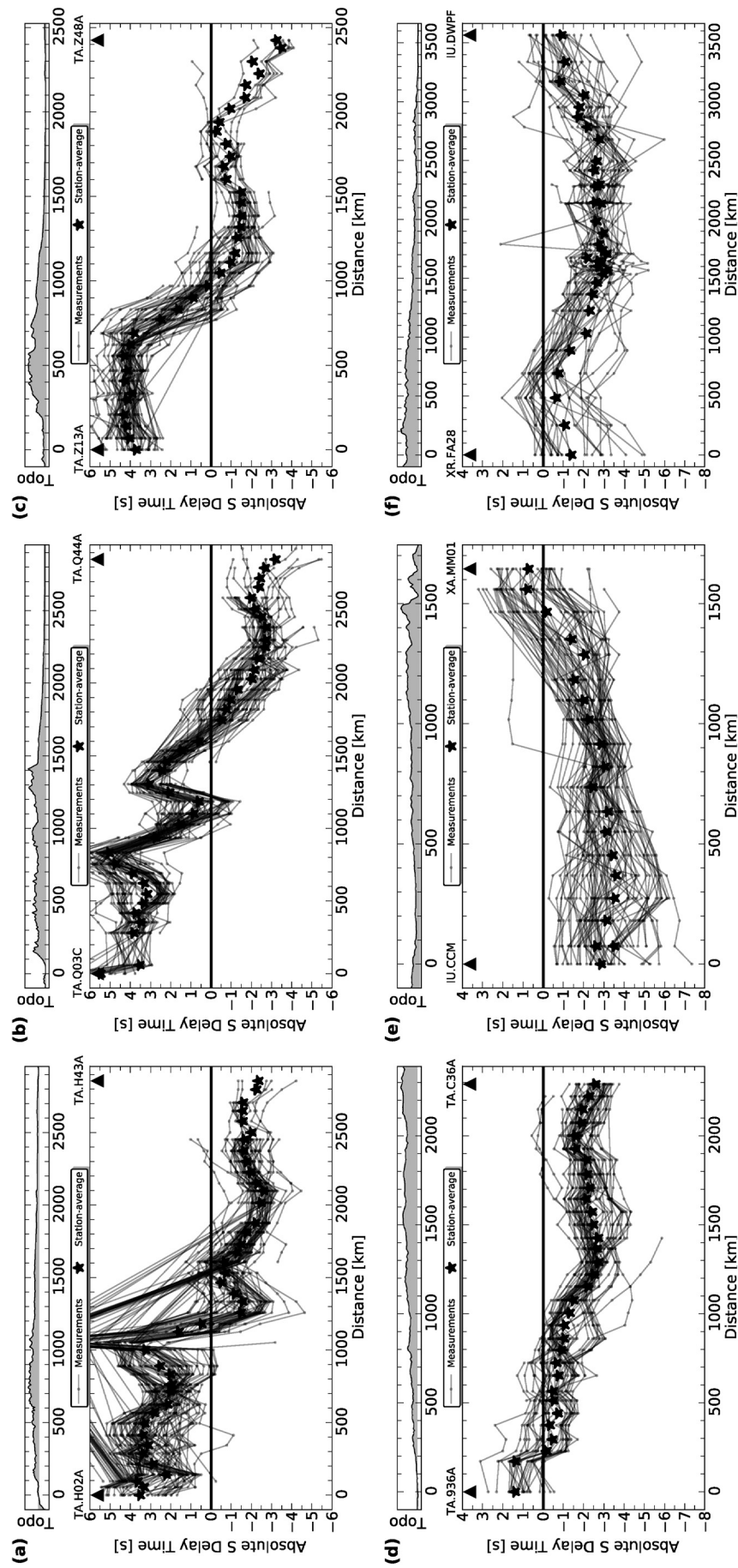


**Fig. 4.** Crust- and event-corrected absolute S delay time variations along 6 profiles surrounding the North American Craton. Delays measured from the same event are connected with solid lines. Station averages are denoted by black stars. Note the extremely high delay at Yellowstone station TA.H17A along the H profile.

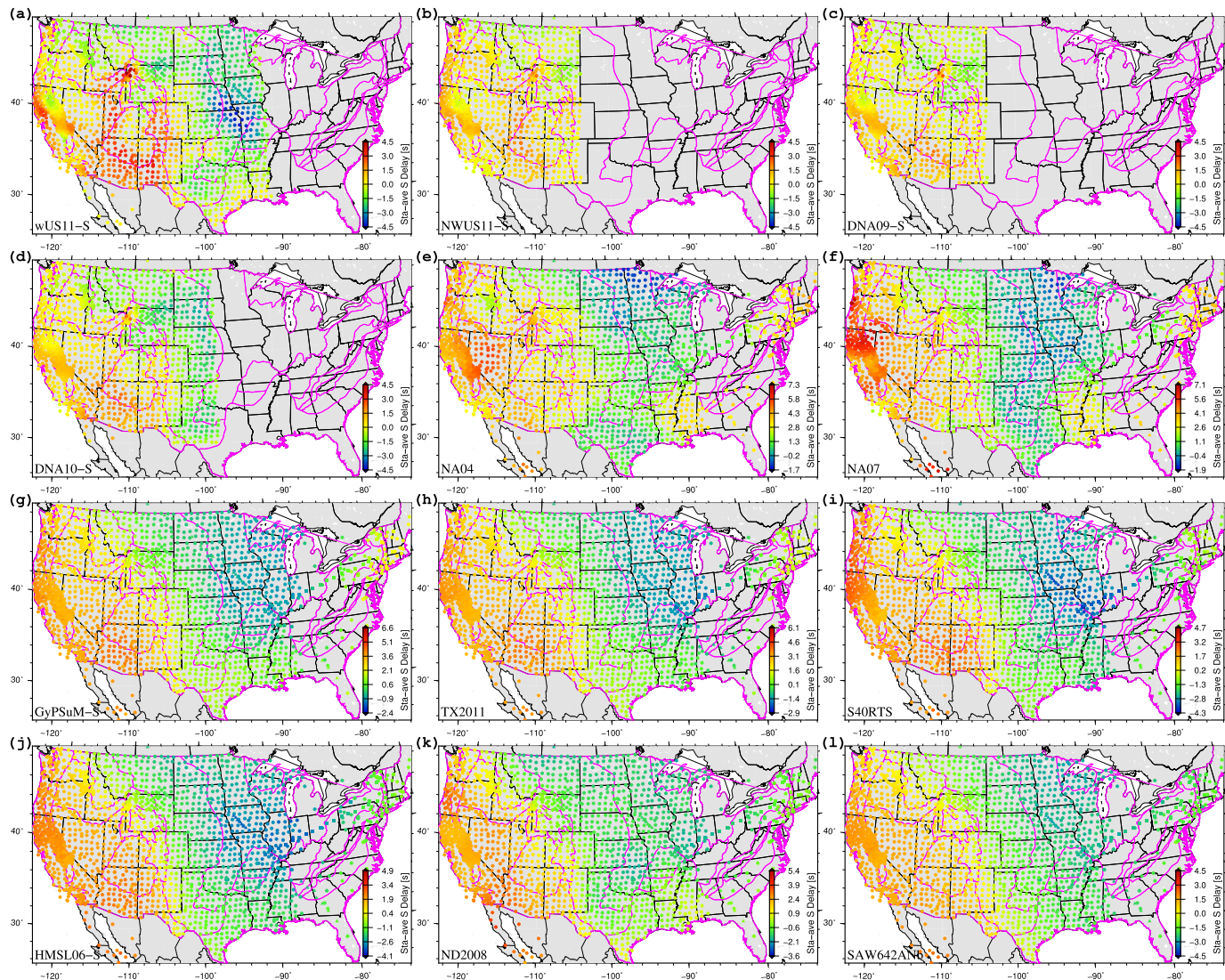


**Fig. 5.** Station-average absolute S delay times predicted by using the ray path geometry from our observations and mantle velocity anomalies from a suite of tomographic models. P delay times are similar to S and are not plotted. These models are regional-scale models DNA09-P and DNA09-S (Obrebski et al., 2010), DNA10-S (Obrebski et al., 2011), NWUS11-P and NWUS11-S (James et al., 2011), wUS11-P and wUS11-S (Schmandt and Humphreys, 2010, 2011), and continental-scale models NA04 (Van der Lee and Frederiksen, 2005), NA07 (Bedle and van der Lee, 2009), GyPSuM-P and GyPSuM-S (Simmons et al., 2010), HMSL06-P and HMSL06-S (Houser et al., 2008), MIT11-P (Burdick et al., 2012), ND2008 (Nettles and Dziewonski, 2008), S40RTS (Ritsema et al., 2011), SAW642ANb (Panning et al., 2010), and TX2011 (Grand, 2002).

Appalachians and Coastal Plain stations), referred to as W-C contrast hereafter. Visually, we used the difference between the Basin and Range and the Central Lowland as a proxy for this contrast.

Models GyPSuM-S and TX2011 are significantly smoother than NA04 and NA07 but also predict about 75% of this large-scale W-C contrast. These two models also predict a similar contrast between the central US and northeastern US (Appalachians and Coastal Plain stations), hereafter referred to as C-NE contrast, as NA04, which is about 50% of the contrast in observed station-side mantle S delays (Fig. 2b). More regionally, the strength and spatial variability of the delays predicted by GyPSuM-S and TX2011 is significantly underestimated. This is also the case for models HMSL06-S, S40RTS, ND2008, and SAW642ANb. The latter two more strongly underestimate the strength of negative delays in the Central Lowland or overestimate the smoothness of mantle structure, thereby largely hiding the C-NE contrast. HMSL06-S and S40RTS also predict 75% of the observed W-C contrast while ND2008 and SAW642ANb predict about half of this contrast. The MIT11-P model predicts only P delays. These predictions are similar to those of GyPSuM-P in the east and DNA09-P in the west.

**Fig. 6** and **Fig. 7** show the means and standard deviations of the predicted delay times for the RMW and RME regions. The standard deviations of the observed S delay times are above 1.6 s for both RMW and RME distributions (**Fig. 7**). Only model wUS11-S predicts a similar standard deviation of 1.5 s for its RMW part. Most models predict standard deviations that are within 0.15 s of each other for the RMW and RME delay time distributions. However, GyPSuM-S, S40RTS, NA04, and wUS11-S predict an up to 0.3 s higher standard deviation for RME, while model ND2008 predicts a 0.3 s lower standard deviation than the other models.

Common to all models is that the major contribution of the difference in *mean delay time* between RMW and RME is incurred within the 80–240 km depth range (**Fig. 6**). The standard deviations in both the RME and RMW predicted delay distribution are also highest in this depth range (**Fig. 7**), suggesting that the 80–240 km layer also hosts strong regional heterogeneity. It is noted that in this depth range one typically finds lithosphere in RME and asthenosphere in RMW. However, even structure in the lower mantle, which is sampled less coherently than shallower structure, contributes to systematic W-E differences, particularly in the global models.

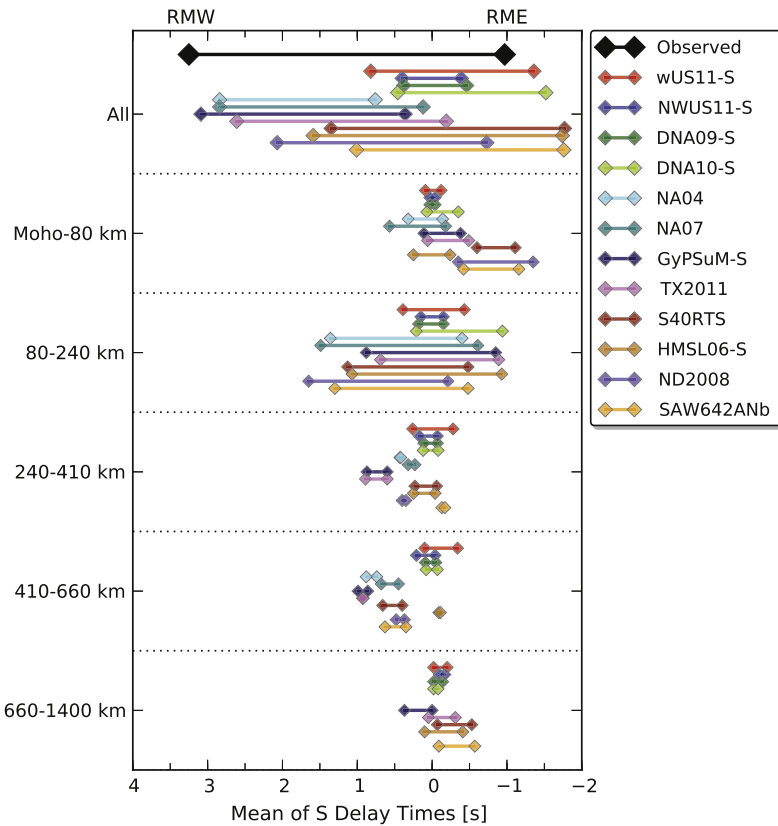


**Fig. 6.** Means of predicted absolute mantle S delay time distributions for RMW and RME stations. Delay times are predicted from structures in a tomographic model's (see model reference in Fig. 5) entire mantle, its Moho-80 km, 80–240 km, 240–410 km, 410–660 km, and 660–1400 km depth ranges. The largest RMW–RME separation in mean delay times is incurred in the 80–240 km depth range, which is predominantly asthenosphere in the west and lithosphere in the east.

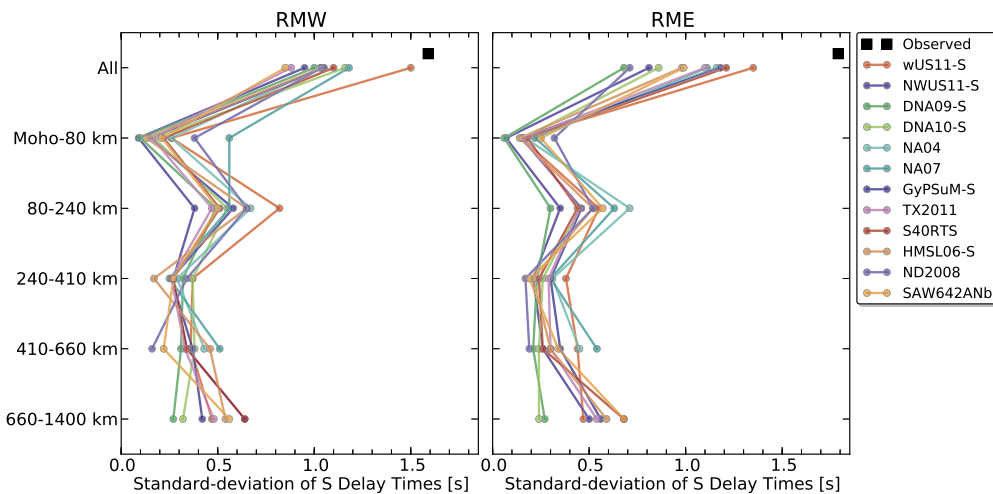


**Fig. 7.** Standard deviations of the same RMW and RME predicted absolute mantle S delay time distributions as in Fig. 6. For both RMW and RME distributions, the largest variance in delay time occurs in the 80–240 km depth range, which is the major contribution to the mantle heterogeneity beneath the US.

#### 4. Conclusions

Crust-and-event-corrected absolute teleseismic *P* and *S* wave delay times measured from seismic waveforms recorded at North American broadband seismic stations show familiar and new patterns of heterogeneity, which includes a 4.2 s *S* delay time difference between the mantles west and east of the Rocky Mountains. This and other patterns are largely consistent with those predicted from a dozen existing tomographic models. However, these models' predictions of the strength of delay times can be further improved. Predicted delay times from these models suggest that structure

from as deep as the lower mantle can contribute to systematic delay time differences at the surface. However, the largest contributions to travel time delays and advances, as well as their variances, are incurred in the 80–240 km depth range, which is predominantly asthenosphere in the west and lithosphere in the east. Thus, heterogeneity in the lithosphere beneath the central and eastern US and in asthenosphere beneath the western US contribute most to the total delay time signatures. The average observed *S* delay difference of 4.2 s between the western and eastern US implies an average 10% or more upper mantle *S* velocity difference down to 240 km. Using larger *S* velocity differences from some tomographic

models would allow for a thinner lithosphere creating similar delay time patterns.

Sharp delay time contrasts are observed across both the Rocky and Appalachian Mountains on the west and east sides. On the south side, the S delay gradient is much more gradual. The delay time contrasts across the Rocky Mountains do not coincide with the mountain front because of the Wyoming craton extending relatively far west and a low-velocity arm separating the Colorado Plateau from the rest of central North America. The S delay changes more rapidly across the Paleozoic Appalachians than the Proterozoic Grenville Province, confirming that lithosphere of the North American Craton extends at least to the Paleozoic Appalachians. Crust-and-event-corrected absolute delays at two stations in Yellowstone National Park are 9 s larger than delays in the central US. This delay time anomaly is far sharper and higher than predicted by any of the evaluated tomographic models.

Predictions of teleseismic S delays from twelve three-dimensional tomographic mantle S velocity models agree generally with observed delay time patterns, but underestimate the delays and advances to varying degrees. Tomographic models derived from different data than teleseismic arrival times predict similarly valid delays as models derived from teleseismic arrivals, while overestimating the smoothness of delay time patterns to varying degrees. Models derived from teleseismic delay times predict the regional variations of delays better but also underestimate the observed absolute delays. Model wUS11-S (Schmandt and Humpreys, 2010, 2011) appears to best predict the S delay observations.

## Acknowledgements

The authors thank the EarthScope (<http://www.earthscope.org>) program, Tony Lowry for providing their Moho model before publishing, and the owners of the tomographic models who provide their models through IRIS EMC (<http://www.iris.edu/dms/products/emc/>) or personal websites and communications. We are thankful to Scott Burdick and an anonymous reviewer for helping us improve the presentation of our findings and to the editor, Peter Shearer, for his considerable help in focusing this paper. Data were obtained through the IRIS DMC (<http://www.iris.edu/dms/dmc/>). Figures were made with GMT (Wessel and Smith, 1998) and Matplotlib (Hunter, 2007). This research was supported by NSF grant EAR-0645752.

## Appendix A. Supplementary material

Supplementary material related to this article can be found online at <http://dx.doi.org/10.1016/j.epsl.2013.11.056>.

## References

- Atwater, T., 1970. Implications of plate tectonics for the Cenozoic tectonic evolution of western North America. *Geol. Soc. Am. Bull.* 81, 3513–3536.
- Atwater, T., 1989. Plate tectonic history of the northeast Pacific and western North America. In: Winterer, E., Hussong, D., Decker, R. (Eds.), *The Eastern Pacific Ocean and Hawaii: The Geology of North America*, vol. N. Geological Society of America, Boulder, CO, pp. 21–72.
- Bally, A., Scotese, C., Ross, M., 1989. North America; Plate-tectonic setting and tectonic elements. In: Bally, A., Palmer, A. (Eds.), *The Geology of North America – An overview: The Geology of North America*, vol. A. Geological Society of America, Boulder, CO, pp. 1–16.
- Bassin, C., Laske, G., Masters, G., 2000. The current limits of resolution for surface wave tomography in North America. *Eos Trans. AGU* 81, F897.
- Bedle, H., van der Lee, S., 2009. S velocity variations beneath North America. *J. Geophys. Res.* 114, B07308. <http://dx.doi.org/10.1029/2008JB005949>.
- Braile, L., Keller, G., Hinze, W., Lidiak, E., 1982. An ancient rift complex and its relation to contemporary seismicity in the New Madrid seismic zone. *Tectonophysics* 1, 225–237. <http://dx.doi.org/10.1016/TC001i002p00225>.
- Burdick, S., van der Hilst, R.D., Vernon, F.L., Martynov, V., Cox, T., Eakins, J., Karasu, G.H., Tylell, J., Astiz, L., Pavlis, G.L., 2012. Model update March 2011: Upper mantle heterogeneity beneath North America from traveltome tomography with global and USArray transportable array data. *Seismol. Res. Lett.* 83, 23–28. <http://dx.doi.org/10.1785/gssrl.83.1.23>.
- Cammarano, F., Goes, S., Vacher, P., Giardini, D., 2003. Inferring upper-mantle temperatures from seismic velocities. *Phys. Earth Planet. Inter.* 138, 197–222. [http://dx.doi.org/10.1016/S0031-9201\(03\)00156-0](http://dx.doi.org/10.1016/S0031-9201(03)00156-0).
- Cara, M., 1979. Lateral variations of S velocity in the upper mantle from higher Rayleigh modes. *Geophys. J. R. Astron. Soc.* 57, 649–670. <http://dx.doi.org/10.1111/j.1365-246X.1979.tb06783.x>.
- Coney, P., Reynolds, S., 1977. Cordilleran Benioff zones. *Nature* 270, 403–406. <http://dx.doi.org/10.1038/270403a0>.
- Dixon, J., Dixon, T., Bell, D., Malservisi, R., 2004. Lateral variation in upper mantle viscosity: role of water. *Earth Planet. Sci. Lett.* 222, 451–467. <http://dx.doi.org/10.1016/j.epsl.2004.03.022>.
- Dziewonski, A., Gilbert, F., 1976. The effect of small, aspherical perturbations on travel times and a re-examination of the corrections for ellipticity. *Geophys. J. R. Astron. Soc.* 44, 7–17. <http://dx.doi.org/10.1111/j.1365-246X.1976.tb00271.x>.
- Engdahl, E., van der Hilst, R., Buland, R., 1998. Global teleseismic earthquake relocation with improved travel times and procedures for depth determination. *Bull. Seismol. Soc. Am.* 88, 722–743.
- Fischer, K.M., Wysession, M.E., Clarke, T.J., Fouch, M.J., Al-Eqabi, G.I., Shore, P.J., Valenzuela, R.W., Li, A., Zaslav, J.M., 1996. The 1995–1996 Missouri to Massachusetts broadband seismometer deployment. *IRIS Newslett.* 15, 6–9.
- Fischer, K.M., Ford, H.A., Abt, D.L., Rychert, C.A., 2010. The lithosphere–asthenosphere boundary. *Annu. Rev. Earth Planet. Sci.* 38, 551–575. <http://dx.doi.org/10.1146/annurev-earth-040809-152438>.
- Frederiksen, A., Bollmann, T., Darbyshire, F., van der Lee, S., 2013. Modification of continental lithosphere by tectonic processes: a tomographic image of central North America. *J. Geophys. Res.* <http://dx.doi.org/10.1002/jgrb.50060>.
- French, S.W., Fischer, K.M., Syracuse, E.M., Wysession, M.E., 2009. Crustal structure beneath the Florida-to-Edmonton broadband seismometer array. *Geophys. Res. Lett.* 36. <http://dx.doi.org/10.1029/2008GL036331>.
- Goes, S., van der Lee, S., 2002. Thermal structure of the North American uppermost mantle inferred from seismic tomography. *J. Geophys. Res.* 107. <http://dx.doi.org/10.1029/2000JB000049>.
- Grand, S., 1994. Mantle shear structure beneath the Americas and surrounding oceans. *J. Geophys. Res.* 99, 11591–11621. <http://dx.doi.org/10.1029/94JB00042>.
- Grand, S., 2002. Mantle shear-wave tomography and the fate of subducted slabs. *Philos. Trans. R. Soc. Lond.* 360, 2475–2491. <http://dx.doi.org/10.1098/rsta.2002.1077>.
- Grand, S.P., Helmberger, D.V., 1984. Upper mantle shear structure of North America. *Geophys. J. R. Astron. Soc.* 76, 399–438. <http://dx.doi.org/10.1111/j.1365-246X.1984.tb0503.x>.
- Hoffman, P., 1988. United Plates of America, The birth of a craton: early Proterozoic assembly and growth of Laurentia. *Annu. Rev. Earth Planet. Sci.* 16, 543–603. <http://dx.doi.org/10.1146/annurev.earth.16.1.543>.
- Houser, C., Masters, G., Shearer, P., Laske, G., 2008. Shear and compressional velocity models of the mantle from cluster analysis of long-period waveforms. *Geophys. J. Int.* 174, 195–212. <http://dx.doi.org/10.1111/j.1365-246X.2008.03763.x>.
- Hunter, J.D., 2007. Matplotlib: A 2D graphics environment. *Comput. Sci. Eng.* 9, 90–95. <http://dx.doi.org/10.1109/MCSE.2007.55>.
- International Seismological Centre, 2010. On-line bulletin. *Int. Seis. Cent. Thatcham, United Kingdom.* <http://www.isc.ac.uk>.
- James, D.E., Fouch, M.J., Carlson, R.W., Roth, J.B., 2011. Slab fragmentation, edge flow and the origin of the Yellowstone hotspot track. *Earth Planet. Sci. Lett.* 311, 124–135. <http://dx.doi.org/10.1016/j.epsl.2011.09.007>.
- Jordan, T.H., 1975. The continental tectosphere. *Rev. Geophys.* 13, 1–12. <http://dx.doi.org/10.1029/RG013i003p00001>.
- Kennett, B., Engdahl, E., 1991. Traveltimes for global earthquake location and phase identification. *Geophys. J. Int.* 105, 429–465. <http://dx.doi.org/10.1111/j.1365-246X.1991.tb06724.x>.
- Lee, D., Grand, S., 1996. Upper mantle shear structure beneath the Colorado Rocky Mountains. *J. Geophys. Res.* 101, 22233–22244. <http://dx.doi.org/10.1029/96JB01502>.
- Lipman, P., 1992. *Magnetism in the Cordilleran United States: Progress and problems.* In: Burchfiel, B., Lipman, P., Zoback, M. (Eds.), *The Geology of North America*, vol. G-3. Geological Society of America, Boulder, CO, pp. 481–514.
- Lou, X., van der Lee, S., Lloyd, S., 2013. AIMBAT: A python/matplotlib tool for measuring teleseismic arrival times. *Seismol. Res. Lett.* 84, 85–93. <http://dx.doi.org/10.1785/0220120033>.
- Lowry, A.R., Pérez-Gussinyé, M., 2011. The role of crustal quartz in controlling Cordilleran deformation. *Nature* 471, 353–357. <http://dx.doi.org/10.1038/nature09912>.
- Lowry, A.R., Becker, T.W., Buehler, J.S., Miller, M.S., Pérez-Gussinyé, M., Schutt, D.L., Seunarine, L.L., 2013. Challenges (and promise) of in-situ lithospheric rheology from isostatic strength analyses. *EGU General Assembly 15. Abstract EGU2013-6248.*
- Nettles, M., Dziewonski, A.M., 2008. Radially anisotropic shear velocity structure of the upper mantle globally and beneath North America. *J. Geophys. Res.* 113. <http://dx.doi.org/10.1029/2006JB004819>.

- Obrebski, M., Allen, R.M., Xue, M., Hung, S.H., 2010. Slab-plume interaction beneath the Pacific Northwest. *Geophys. Res. Lett.* 37. <http://dx.doi.org/10.1029/2010GL043489>.
- Obrebski, M., Allen, R.M., Pollitz, F., Hung, S.H., 2011. Lithosphere–asthenosphere interaction beneath the western United States from the joint inversion of body-wave traveltimes and surface-wave phase velocities. *Geophys. J. Int.* 185, 1003–1021. <http://dx.doi.org/10.1111/j.1365-246X.2011.04990.x>.
- Owens, T., Crotwell, H., Groves, C., Oliver-Paul, P., 2004. SOD: Standing order for data. *Seismol. Res. Lett.* 75, 515–520. <http://dx.doi.org/10.1785/gssrl.75.4.515-a>.
- Panning, M.P., Lekic, V., Romanowicz, B.A., 2010. Importance of crustal corrections in the development of a new global model of radial anisotropy. *J. Geophys. Res.* 115. <http://dx.doi.org/10.1029/2010JB007520>.
- Pavlis, G.L., Sigloch, K., Burdick, S., Fouch, M.J., Vernon, F.L., 2012. Unraveling the geometry of the Farallon plate: Synthesis of three-dimensional imaging results from USArray. *Tectonophysics* 532, 82–102. <http://dx.doi.org/10.1016/j.tecto.2012.02.008>.
- Ritsema, J., Deuss, A., van Heijst, H.J., Woodhouse, J.H., 2011. S40RTS: a degree-40 shear-velocity model for the mantle from new Rayleigh wave dispersion, teleseismic traveltimes and normal-mode splitting function measurements. *Geophys. J. Int.* 184, 1223–1236. <http://dx.doi.org/10.1111/j.1365-246X.2010.04884.x>.
- Roth, J.B., Fouch, M.J., James, D.E., Carlson, R.W., 2008. Three-dimensional seismic velocity structure of the northwestern United States. *Geophys. Res. Lett.* 35. <http://dx.doi.org/10.1029/2008GL034669>.
- Rychert, C.A., Rondenay, S., Fischer, K.M., 2007. P-to-S and S-to-P imaging of a sharp lithosphere–asthenosphere boundary beneath eastern North America. *J. Geophys. Res.* 112. <http://dx.doi.org/10.1029/2006JB004619>.
- Schmandt, B., Humphreys, E., 2010. Complex subduction and small-scale convection revealed by body-wave tomography of the western United States upper mantle. *Earth Planet. Sci. Lett.* 297, 435–445. <http://dx.doi.org/10.1016/j.epsl.2010.06.047>.
- Schmandt, B., Humphreys, E., 2011. Seismically imaged relict slab from the 55 Ma Siletzia accretion to the northwest United States. *Geology* 39, 175–178. <http://dx.doi.org/10.1130/G31558.1>.
- Sigloch, K., Mihalynuk, M.G., 2013. Intra-oceanic subduction shaped the assembly of Cordilleran North America. *Nature* 496, 50–56. <http://dx.doi.org/10.1038/nature12019>.
- Sigloch, K., McQuarrie, N., Nolet, G., 2008. Two-stage subduction history under North America inferred from multiple-frequency tomography. *Nat. Geosci.* 458–462. <http://dx.doi.org/10.1038/ngeo231>.
- Simmons, N.A., Forte, A.M., Boschi, L., Grand, S.P., 2010. GyPSuM: A joint tomographic model of mantle density and seismic wave speeds. *J. Geophys. Res.* 115. <http://dx.doi.org/10.1029/2010JB007631>.
- Stock, J., Molnar, P., 1988. Uncertainties and implications of the late cretaceous and tertiary position of North America relative to the Farallon, Kula, and Pacific plates. *Tectonics* 7, 1339–1384. <http://dx.doi.org/10.1029/TC007i006p01339>.
- Tian, Y., Sigloch, K., Nolet, G., 2009. Multiple-frequency SH-wave tomography of the western US upper mantle. *Geophys. J. Int.* 178, 1384–1402. <http://dx.doi.org/10.1111/j.1365-246X.2009.04225.x>.
- Tian, Y., Zhou, Y., Sigloch, K., Nolet, G., Laske, G., 2011. Structure of North American mantle constrained by simultaneous inversion of multiple-frequency SH, SS, and Love waves. *J. Geophys. Res.* 116. <http://dx.doi.org/10.1029/2010JB007704>.
- Van der Lee, S., Frederiksen, A., 2005. Surface wave tomography applied to the North American upper mantle. In: Levander, A., Nolet, G. (Eds.), *Seismic Earth: Array Analysis of Broadband Seismograms*. In: *Geophys. Monogr.*, vol. 157. AGU, Washington, DC, pp. 67–80.
- Van der Lee, S., Nolet, G., 1997a. Seismic image of the subducted trailing fragments of the Farallon plate. *Nature* 386, 266–269. <http://dx.doi.org/10.1038/386266a0>.
- Van der Lee, S., Nolet, G., 1997b. Upper mantle S velocity structure of North America. *J. Geophys. Res.* 102, 22815–22838. <http://dx.doi.org/10.1029/97JB01168>.
- Van der Lee, S., Regenauer-Lieb, K., Yuen, D.A., 2008. The role of water in connecting past and future episodes of subduction. *Earth Planet. Sci. Lett.* 273, 15–27. <http://dx.doi.org/10.1016/j.epsl.2008.04.041>.
- Van Schmus, W., Hinze, W., 1985. The midcontinent rift system. *Annu. Rev. Earth Planet. Sci.* 13, 345–383. <http://dx.doi.org/10.1146/annurev.earth.13.1.345>.
- VanDecar, J., Crosson, R., 1990. Determination of teleseismic relative phase arrival times using multi-channel cross-correlation and least squares. *Bull. Seismol. Soc. Am.* 80, 150–169.
- Wessel, P., Smith, W.H.F., 1998. New, improved version of generic mapping tools released. *Eos Trans. AGU* 79, 579. <http://dx.doi.org/10.1029/98EO00426>.
- Whitmeyer, S.J., Karlstrom, K.E., 2007. Tectonic model for the Proterozoic growth of North America. *Geosphere* 3, 220–259. <http://dx.doi.org/10.1130/GES00055.1>.
- Wysession, M.E., Fisher, K.M., Al-eqabi, G.I., Shore, P.J., 2000. From MOMA to FLED: Designing North American broadband arrays. *Eos Trans. AGU*, Spring Meeting Suppl. S317.